2010 IEEE International Conference on Multisensor Fusion and Integration for Intelligent Systems
University of Utah, Salt Lake City, UT, USA, Sept. 5-7, 2010

Multiscale Adaptive Sampling In Environmental Robotics

Vadiraj Hombal, Arthur Sanderson and D. Richard Blidberg

***Abstract*— Observation of spatially distributed oceanographic phenomena using sensor-enabled AUVs involves a trade-off between coverage and resolution. In this paper the performance of adaptive variation sensitive sample distributions in such a sensing task is evaluated under mission constraints such as finite measurement time and finite vehicle speed and compared to uniform sampling. The relative performance of the four algorithms considered is characterized in terms of localization of features in the test functions.**

I. INTRODUCTION

This work is concerned with the observation and monitoring of environmental processes that occur in oceans and other waterbodies. Such processes are typically non-stationary, and vary at multiple spatial and temporal scales [9], [11]. Observation of such processes, requires sustained, pervasive sensing at appropriate spatial and temporal resolutions. While sensing modes such as satellite imagery yield high resolution snapshots of the ocean surface, subsurface sensing of oceanographic processes can only be achieved through *in-situ* sensing using mobile sensor platforms, such as AUVs [1], [2], [5], [6], [8], [10].

The objective of oceanographic observation is the recovery of the apriori unknown spatio-temporal distribution of an oceanographic process $f(x,t)$, $x \in \Omega$, $t \in [0,T]$, that varies continuously in space and time. The goal is to obtain an estimate, $\hat{f}(x,t)$, of the underlying distribution based on space-time point sample data collected over the domain Ω of area $A \triangleq |\Omega|$, and over a period of T days [12], [13]. Collection of such data involves visiting each sample location in order and measuring the underlying function. Hence realization is not instantaneous and is instead spread over an interval, T_s [7], [9]. In this paper, the underlying process is assumed to be stationary during the interval Δt and recovery over an interval $T = n\Delta t$, is achieved by recovering a series of n 'snapshots' taken Δt apart. In addition, a nominal value for spatial resolution, Δx is assumed. The aim is to obtain samples at this resolution such that *features* represented by the variability in the distribution are sufficiently resolved. In general, these features represent the variability within a distribution, and Δx and Δt are chosen so as to resolve this variability at a level of discretization that is of interest in analysis. Δx and Δt maybe referred to as *process constraints*, since they represent the sampling requirements associated with the variability in the underlying distribution.

In addition, observation of such processes is subject to *resource constraints* such as the finite speed of the vehicle, limited amount of on-board energy, and finite sample rate of the sensors that limit the ability to realize sensing tasks at the resolution desired. Specifically, the total energy available on-board the vehicle for navigation and measurement purposes is, $E_s \leq E_{\max} < \infty$.

Under these constraints, the problem of estimation of spatio-temporal distributions using space-time point samples, realized using mobile sensing platforms may be written as:

$$\begin{aligned} \text{minimize} \quad & I(X_s) = \int_{\Omega} \|f(x) - \hat{f}\,(x|Z_s)\| \mathbf{dx} \\ \text{such that} \quad & T_s \leq \Delta t, \quad E_s \leq E_{\max} \end{aligned}$$

where $Z_s = \{f(\mathbf{x}_i), \mathbf{x}_i\}_{i=1}^{k}$ is the data set associated with the sample distribution. A low value of $I(X_s)$ indicates high fidelity between the underlying function, f and its reconstruction, $\hat{f}$, and the quality of reconstruction depends on the number and location of the sample points.

In this paper we assume that number of sample points, N_s is fixed by a sample budget and focus on the distribution of sample locations, X_s. Since the underlying function, $f(x)$, is not apriori known, the optimal X_s cannot be selected apriori, and must instead be sequentially identified based on information contained in intermediate samples. Towards this in previous work adaptive sampling algorithms that use hierarchical error based surrogate models with localized sampling was proposed [4]. These sequential multiscale adaptive sampling algorithms(MSAS) were shown to achieve a variation sensitive sampling distribution through variation sensitive modeling of the underlying function. However, in MSAS, the sample selection was based purely on quality of reconstruction and not dependent on realization costs. In this paper the MSAS is augmented with a path planning step and the sequential variation sensitive sample distributions generated by MSAS are evaluated for their realization costs under the constraints such as finite vehicle speed and finite measurement time. The performance of the algorithms is compared and contrasted with two different realizations of the uniform sample distribution.

Funding was provided by grant numbers IIS-0329837 and NSF EEC-0812056 from the National Science Foundation and by the Office of Naval Research (ONR) under grants #N00014-04-1-0264, #N00014-03-C-0109, #N00014-02-1-008.

Vadiraj Hombal is with the Department of Civil & Environmental Engineering, Vanderbilt University, Nashville, TN 37221, USA vadiraj.hombal@vanderbilt.edu

Arthur Sanderson is with Faculty of Electrical, Computer & Systems Engineering, Rensselaer Polytechnic Institute, Troy, NY 12180, USA sandea@rpi.edu

D. Richard Blidberg is with Autonomous Undersea Research Institute (AUSI), Lee, New Hampshire 03861, USA blidberg@ausi.org

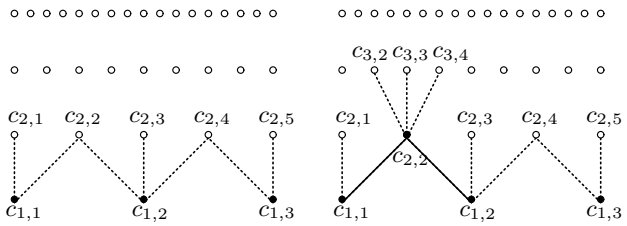

(a) Iteration 1 (b) Iteration 2

Fig. 1: Mechanics of the MSAS Algorithm

II. Multi Scale Adaptive Sampling (MSAS)

A brief introduction of MSAS is provided here. For details see [4]. Multi Scale Adaptive Sampling algorithm is based on a hierarchical decomposition of the approximation error using a multilayered hierarchy of Radial Basis Function Networks (RBFN) of different scales to generate a coarse to fine representation of a given function. In MSAS, the structural parameters are set according to an ordering imposed by a hierarchical *analysis grid* defined on the problem domain, Ω. MSAS algorithms traverse the analysis grid and arrive at a sparse representation of an a-priori *unknown* function through sequential discovery of significant bases in the grid. In each iteration, the selection of a node for refinement and modeling is based on criteria that use information contained in residues, which represent a sampling of the true approximation error in the current function estimate.

Procedurally, MSAS implements a *select-refine-model* cycle presented below:

1. **select node** from the set of allowable candidate nodes
2. **sample function** at child nodes of the selected node
3. **add** the **basis** of the selected node to the model
4. **add children** of the modeled node to the set of allowable candidate nodes
5. **repeat** till some termination criteria is met

These ideas are illustrated in Figure 1. In Fig 1a, nodes C_1 correspond to previously modeled nodes, ϕ_1 which correspond to $\hat{f}_1 = \Phi_1 \mathbf{w}_1$. Nodes C_2, which form the set of all un-modeled children of the previously modeled nodes, form the set of allowable candidate nodes for the next iteration. Suppose node $c_{2,2}$ is selected for modeling in the next iteration. The selected node $c_{2,2}$ is first refined by taking measurements at the locations of the child nodes $\{c_{3,2}, c_{3,3}, c_{3,4}\}$, and is then introduced into the model: $\hat{f}_2 = \hat{f}_1 + \Phi_{2,2} w_{2,2}$. Modeling of the selected node $c_{2,2}$ introduces the child nodes into the set of allowable nodes for the next iteration. Thus, as seen in Fig 1b, the set of allowable candidate nodes is $\{C_1 \setminus c_{2,2}\} \cup \{c_{3,2}, c_{3,3}, c_{3,4}\}$.

The mechanism described above allows for traversal of the scale space grid down to an arbitrary grid depth with arbitrarily high sampling resolution via refinement. In MSAS, the maximum allowable sampling rate is assumed to correspond to the highest resolution of the grid and the maximum sample size, $N_{\max}$, is assumed to be less than 2^M, where M is the highest grid level.

In MSAS information contained in these residues is directly employed in each iteration to select a node, c^*_{i+1} from the set A_C. Two selection criteria are presented: 1) greatest residue and 2) weighted threshold: 1) In MSAS algorithm based on greatest residue (MSAS-GR), the node corresponding to the greatest residue is selected from the set of allowable candidate nodes for modeling in the next iteration, and 2) In MSAS algorithm based on weighted threshold (MSAS-wTH), the residues are first weighted by the scale of the corresponding bases and all nodes in the set A_c with weighted residue greater than average weighted residue in A_c are selected.s

A. Path Planning With Augmented MSAS

In order to facilitate sequential realization of the MSAS sample distribution the *refinement* step in MSAS is augmented with a *path-planning* step. The *path-planning* step takes the sample points identified by the *refinement* step as an input, and generates an efficient path through them to be followed by the vehicle, such that the distance traveled is minimized. As is demonstrated in subsequent sections, in contrast to the energy minimizing sequencing of LM, MSAS algorithm augmented with a path planning module represents a sample sequence that maximizes the reduction in reconstruction error per sample.

In each iteration of MSAS, using the information contained in the residues, the selection step imposes an ordering on all the nodes in the set of allowable candidate nodes C_A. These nodes in turn represent the various regions of the domain that are eligible for refinement in the next iteration. Then, according to the selection criterion implemented, the selection step then identifies critical node(s) which must be introduced into the model in the next iteration. Refinement of these selected nodes, generates the corresponding *sample distribution*. The path-planning step takes this sample distribution as an input and generates a *sampling sequence* that imposes an ordering on the distribution so as to minimize the distance traveled during its realization.

The selection and path-planning functions are distinct. Selection of critical regions for refinement does not depend on the expected energy expenditure in actual realization. Reduction in energy expenditure is achieved subsequent to selection (in the planning step) by imposing a distance minimizing order on the sample distribution.

III. Preliminaries

A *sample distribution* $X_s \triangleq \{\mathbf{x}_1, \mathbf{x}_2, ...\mathbf{x}_k : \mathbf{x}_i \in \Omega\}$ is a set of k pairwise distinct elements, $\mathbf{x}_i$, each of which represents a candidate sample location where the underlying function is to be sampled by measuring its value. A *sampling sequence*, $X_\lambda \triangleq (\mathbf{x}_{\lambda_1}, \mathbf{x}_{\lambda_2}, ...\mathbf{x}_{\lambda_k})$, $\mathbf{x}_{\lambda_i} \in X_s$, $|X_\lambda| = |X_s|$, is an ordering on the elements in X_s which induces a length property on the distribution:

$$L_\lambda(X_s) = \sum_{i=1}^{k-1} \|x_{\lambda_i} - x_{\lambda_{i+1}}\|. \quad (1)$$

The sample locations in the set X_s are to be visited in the order specified by the corresponding sample sequence, X_λ. Thus the length of a distribution depends on the choice of the sequence imposed on it. For a given distribution there is more than one sequence that assigns the same length on the distribution. A *sampling mission* consists of realization of a sample distribution, X_s, by visiting locations $\mathbf{x}_i \in X_s$ according to the ordering in X_λ and sampling the underlying function. The corresponding mission time may be written as:

$$T_\lambda = \frac{L_\lambda(X_s)}{v} + k\tau_m = \sum_{i=1}^{k-1} \|x_{\lambda_i} - x_{\lambda_{i+1}}\| \times \frac{1}{v} + k\tau_m \ \leq \Delta t \tag{2}$$

where $\tau_m \geq 0$ is the measurement time at a sample location and is assumed to be the same at all sample locations. $v > 0$ is the nominal speed of the vehicle during the mission. The energy consumed in the mission is given by [14]:

$$E_\lambda = \left(\alpha v^3 + \beta\right) T_\lambda \ \leq E_{\max} \tag{3}$$

where α is a constant describing the vehicle's hydrodynamic properties, β is the hotel load. Thus apart from requiring time $k\tau_m$, the number of samples taken, k, also constrains E_λ since it increases hotel load and reduces energy available for transit.

The variables in the equations defining mission time and energy may be classified into three groups: 1) parameters α and β represent *vehicle* characteristics which define the capabilities of the vehicle, 2) the vehicle speed, v, and measurement time, τ_m, represent the *mission* characteristics and, 3) parameters L_λ and k represent the *sample* characteristics.

For a given vehicle and sensor, *mission characteristic*, $\kappa = v \times \tau_m$, is assumed fixed. It is assumed that vehicles are operated at an average speed $v \leq v_{\max}$ such that utlilization of on-board energy is optimized and that each measurement takes a fixed time τ_m.

A sample distribution is characterized by: 1) the amount of information contained in it, and 2) the energy expenditure incurred in its realization. In this work, the amount of information contained in a sample distribution is measured as a function of error in reconstruction of the underlying function. The focus is on evaluating the impact (in terms of reconstruction error) of the sample characteristics on the realization of the sample distributions generated by different algorithms. Since for a given vehicle and mission profile, the energy consumed is proportional to the time taken, evaluation of energy consumption is addressed via the evaluation of the corresponding mission time which, in turn depends on L_λ and N_λ.

IV. Path Plan Evaluation

In the rest of this paper the performance of GR and wTH is evaluated based on their sequential properties such as the number of samples required, the distance traveled, and the time taken time taken to achieve a given percentage of error and compared to the Lawnmower(LM) sequence and Sequential Refinement(SR), which are two non-adaptive sampling regimes. This evaluation is based on six test functions. The functional forms of five of the test functions are given below:

$$\begin{aligned}
f_1(x,y) &= 2e^{-5\left(0.5(x-1.2)^2+2y^2\right)} \\
f_2(x,y) &= \text{erf}(x-.3) + 2\text{erf}(y-2.21) \\
f_3(x,y) &= f_1(x,y) + f_2(x,y) \\
f_4(x,y) &= \texttt{peaks}(x,y) \\
f_5(x,y) &= -0.4\tanh\left(50(x-0.13)(y-1.13)\right) + 0.6
\end{aligned}$$

where `peaks` is a MATLAB function. The sixth test function is the salinity distribution data generated by the three dimensional Estuarine Coastal Ocean Model (ECOM-3D for the Tampa Bay Coastal Prediction System (CPS) [3] (Courtesy of M. Luther, USF). All the functions have been renormalized to $\Omega = [-4,4]^2$. The maximum sampling resolution is set to $(b-a)/2^M \times (b-a)/2^M = 0.0625$sq. units, with $M = 5$. Thus the set of possible sample locations for all the algorithms consists of $(2^M+1)^2 = 1089$ samples. Of these, 25 samples of the initial bootstrap iteration of MSAS are available to all algorithms at initialization. These 25 samples maybe assumed to be obtained through a network of static nodes and thus no measurement or travel cost is assigned to them. The set of possible samples consists of the remaining 1064 samples, and is available to all algorithms. The differences between the sequences generated by the various algorithms are induced due to the order in which the algorithms select these samples.

A. Critical and Redundant Regions

The functions listed above are selected as representatives of functions with different level of localization of features within the domain. In order to quantify localization, we consider a partition of the domain, Ω into critical and redundant regions:

$$\begin{aligned}
\Omega_R &= \left\{(x,y) \in \Omega : |\nabla^2 f(x,y)| < \epsilon\right\} \text{(Redundant)} \\
\Omega_C &= \left\{(x,y) \in \Omega : |\nabla^2 f(x,y)| \geq \epsilon\right\} \text{(Critical)}
\end{aligned}$$

where $\nabla^2 f$ is the Laplacian of f, $\epsilon \geq 0$ and $\Omega = \Omega_C \cup \Omega_R$. Thus, Ω_C and Ω_R represent regions of large variation and small variation respectively. Intuitively, regions of the domain where the function is constant or varies at a fixed rate are classified as redundant regions. Since variation within this region may be represented by a first order approximation based on samples at the boundaries of such regions, and samples in the interior of these regions don't add to the approximation, these samples may be termed redundant. However, they account for exploratory samples in the discovery of the a-priori unknown feature.

The *localization index* $\mathcal{L} \in [0,1]$ is defined as: $\mathcal{L} \triangleq \frac{|\Omega_C|}{|\Omega|}$ where, $|\cdot|$ denotes size of a region. A low value of $\mathcal{L}$ indicates a function whose features are localized in the domain, while a high value indicates a function with features diffused across the domain. Localization index is a measure of the relative size of the feature, but it does not capture the spread of the feature. The *spread* of a function may be quantified by a

	f_1	f_2	f_3	f_4	f_5	f_6
$\mathcal{L}$	0.0591	0.5646	0.5925	0.4789	0.0819	0.7671
$\mathcal{R}$	0.0657	1.0000	1.0000	0.6833	1.0000	1.0000
$\mathcal{C}$	132.23	7.22	119.13	122.69	175.64	23.75
	Qualitative					
$\mathcal{L}$	Low	Medium	Medium	Medium	Low	High
$\mathcal{R}$	Low	High	High	Medium	High	High
$\mathcal{C}$	High	Low	Medium	Medium	High	Low

TABLE I: Quantitative and Qualitative Description of Localization in Test Functions

measure $\mathcal{R} \in [0, 1]$ defined as:

$$\mathcal{R} \triangleq \frac{\text{range}(\Omega_C)}{\text{range}(\Omega_R)}.$$

Similarly the separation between the critical regions and the redundant regions in the *feature* space may be quantified by a measure $\mathcal{C} \geq 1$ defined as:

$$\mathcal{C} \triangleq \frac{\max\{|\nabla^2 f(x,y)| \ : (x,y) \in \Omega_C\}}{\max\{|\nabla^2 f(x,y)| \ : (x,y) \in \Omega_R\}}.$$

A low value of the measure $\mathcal{C}$ indicates absence of any pronounced features in the domain (f_2 and f_6) since the maximum variation in critical and redundant regions are of similar maginitudes.

$(\mathcal{L}, \mathcal{R}, \mathcal{C})$, provide a measure of the localization of a test function, that is reasonable for the discussion here. The quantitative and qualitative values for the six test functions are shown in Table I. The six test functions represent a fair sampling of the $(\mathcal{L}, \mathcal{R}, \mathcal{C})$ space. Of these, functions f_1(Low, Low, High), f_4 (Medium, Medium, High) and f_6 (High, High, Low) will be used for illustrations.

It is noted here that these measures are employed ex post facto for evaluation purposes only. They do not influence the selection process in MSAS.

B. Evaluation of Distance Traveled and Sample Rates

In this section, the algorithms are evaluated in terms of sample characteristics, namely, number of samples taken, N_s, and the distance traveled, L_s.

1) Lawnmower Sampling (LM): The shortest tour between all the $(2^M + 1)^2 - 25$ sample points is achieved by following the LM sampling sequence through them (Fig. 2a). LM sampling has a tour length $L_s \sim (2^M + 2)$ units and an average distance traveled per sample $\sim 2^{-M}$ (See Table II). Thus for a given number of samples, LM is optimal in terms of distance traveled. If the measurement time per sample (τ_m) is insignificant when compared to transit costs and if sufficient time is available to cover the domain then, LM sampling is expected to be an efficient sampling design in terms of energy costs.

However, in practice, the size of the domain and the energy constraints are typically such that the time available (Δt) for mission is less than the time it takes to cover the domain using LM sampling. LM sampling of the entire domain at the highest resolution is not feasible due to the constraints. A compromise is then made, and either the domain or the resolution is reduced to satisfy the constraints. The two non-adaptive sampling algorithms evaluated here are representatives of these compromises. LM represents the effect of loss of coverage, while SR represents the effect of loss of resolution.

	wTH	GR	SR	LM
f_1	0.49	1.38	0.46	0.26
f_2	0.47	1.35	0.46	0.26
f_3	0.48	1.41	0.46	0.26
f_4	0.50	1.50	0.46	0.26
f_5	0.49	1.34	0.46	0.26
f_6	0.47	1.39	0.46	0.26

TABLE II: Distance Traveled Per Sample

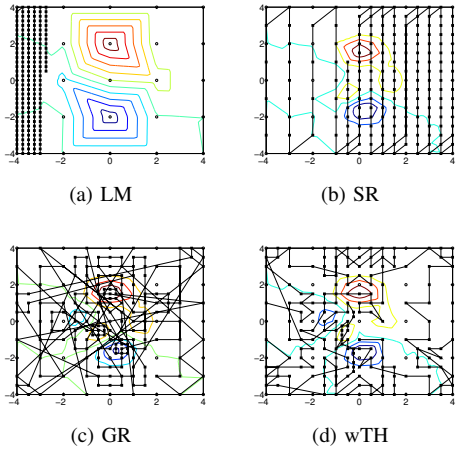

(a) LM (b) SR (c) GR (d) wTH

Fig. 2: Sample Distributions and Trajectories. f_4, $N_s = 200$. $L_s^{\text{LM}} \approx 57$, $L_s^{\text{SR}} \approx 174$, $L_s^{\text{GR}} \approx 283$, $L_s^{\text{wTH}} \approx 160$.

In addition, LM suffers from a *sample latency* due to slow rate of discovery of samples that contribute to reconstruction. In the error vs. number of samples characteristic shown in Fig.s 3a, 3c, and 3d this latency manifests as concave segments. In the case of f_1, this latency is due to fact that, until 500 samples, the sampling sequence does not reach the critical feature region which contains all measurements that are significant for reconstruction. After about 500 samples, when the sequence arrives at the critical region, the reconstruction error decreases rapidly. However, even with non-localized functions such as f_6, where critical regions are encountered early on, latency cannot be avoided (Fig. 3d). Due to this latency, the number of samples required to achieve a given level of error is very large for LM. The principal effect of this latency is that it makes LM highly sensitive to measurement costs and thus, in a practical setting, any advantage due to optimal travel costs is offset by the slow rate of discovery.

2) Successive Refinement (SR): The latency inherent in LM sampling may be reduced by a non-adaptive multi-stage uniform sampling algorithm in which at each stage, k, the sample set corresponds to the location of the k^{th}-layer nodes of the analysis grid (Fig. 2b). At each stage, the vehicle still travels in a lawnmower pattern and the total tour length $L_s \sim 2^{M+1} + 2M - 12$.

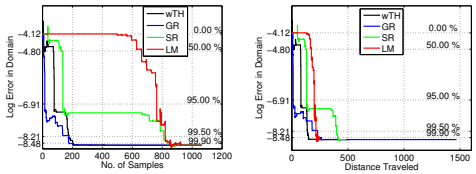

(a) f_1 Error Vs. N_s (b) f_1 Error Vs. L_s

(c) f_4 Error Vs. N_s (d) f_4 Error Vs. L_s

(e) f_6 Error Vs. N_s (f) f_6 Error Vs. L_s

Fig. 3: Reconstruction Error Vs Number of Samples and Distance Traveled

By employing multi-stage refinements, the SR allows for non-adaptive coarse-to-fine sampling of the domain. SR divides the latency into stages and thus increases the learning rate when compared to LM. Especially with non-localized functions such as f_6, this coarse to fine learning is effective (Fig. 3c,d) in terms of number of samples.

3) MSAS-GR: As seen in Fig. 3 by considering only the node with the greatest residue for refinement, GR achieves a given error level with the least number of samples amongst the algorithms considered. This holds even for non-localized functions such as f_6. In the case of localized functions such as f_1, MSAS offers significant savings in the number of samples required to achieve the lowest possible error.

However, in searching for the node with the highest residue in each iteration, GR makes long excursions across the domain (Fig. 4). Consequently, GR has large distance traveled per sample (Table II). For localized functions, these high travel costs are incurred while acquiring measurements in the redundant regions. As seen in Fig. 2c, long diagonal excursions are made between nodes on the boundaries. In contrast, tours in the critical region are relatively short.

C. MSAS-wTH

By selecting more than one node, wTH shares travel costs between nodes, the distance traveled per sample is comparable to SR sampling (Table II) and the error rate faster than SR sampling (Fig. 3). Since multiple nodes are selected in each iteration, wTH is suboptimal to GR and some amount of latency is induced since wTH selects more samples in redundant region than GR (Fig. 2d).

D. Sample Efficiency

In general, MSAS algorithms sample the critical region at a higher rate than uniform sampling even for non-localized functions such as f_6 (Fig. 5) . Further, while for non-localized functions the sample rates required to fully resolve critical region are comparable, in the case of localized functions, MSAS algorithms afford significant savings in the number of samples required to fully resolve the critical regions. As a consequence of this, for a given number of samples, MSAS algorithms allow for reconstructions of much higher quality algorithms when compared to LM and SR. The 256-sample distribution and the corresponding reconstruction for functions, f_1, f_4 and f_6 is shown in Fig. 6.

V. Effect of Finite Vehicle Speed and Measurement Time

In this section the performance algorithms in terms of mission time is evaluated. As discussed in the previous section, the relative performance of the algorithms in terms of the sample characteristics interact to have practical consequences on the realization of sample sequences generated by the algorithms. It is assumed that the sampling missions are characterized by vehicles with finite speed, $v > 0$ and measurement times, $\tau_m \geq 0$. To begin, two limiting cases of the mission characteristic, $\kappa \triangleq v * \tau_m$, $\kappa \in [0, \infty)$ are considered: 1) $\kappa \to \infty$ and, 2)$\kappa = 0$.

A. Limiting Case 1: $\kappa \to \infty$

When $v \to \infty$, then $\kappa \to \infty$ represents the scenario where measurement costs dominate travel costs as the entire mission time consists of the τ_m. The error vs number of samples performance described in previous section characterizes this case. As discussed in that section, in such cases, MSAS dominates LM and SR. While no physical oceanographic deployments are possible under these assumptions, the characterization of the performance of algorithms under these conditions has important bearing on the feasibility of the algorithms as viable sampling strategies under more realistic scenarios. This is discussed in subsequent sections.

B. Limiting Case 2: $\kappa = 0$

The $\tau_m = 0$, $\kappa = 0$ mission represents the case of instantaneous sampling. In this case the travels costs dominate. Since, $\tau_m = 0$, in effect, reconstruction error vs mission time curve, assuming $v = 1$, is the same as the error vs distance traveled performance in Fig. 3. Since this is the base scenario on which further analysis is conducted, a detailed explanation of the relative performance of the algorithms is presented. Since LM sampling sequence has the lowest distance traveled per sample, the time required by LM to cover the grid, T^{LM}, is smallest. As a result, for functions with medium to high $\mathcal{R}^1$, *provided* $T^{\text{LM}} < \Delta t$, LM is an efficient sampling sequence to achieve high resolution reconstruction by capturing a high percentage of the error.

[1]Functions with a significant spread of the features. For these functions coverage is critical.

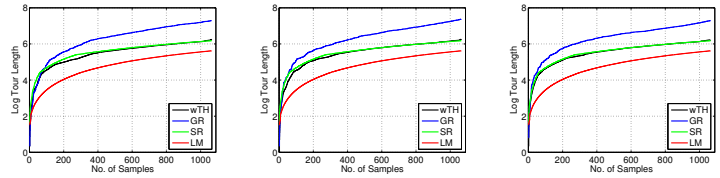

(a) f_1 Distance Traveled (b) f_4 Distance Traveled (c) f_6 Distance Traveled

Fig. 4: Number of Samples Vs. Logarithm of Distance Traveled

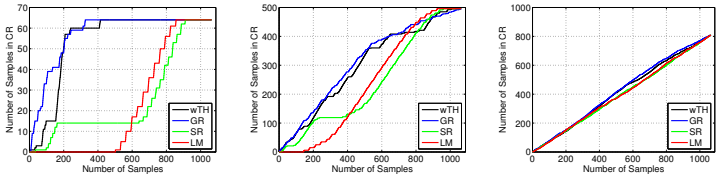

(a) f_1 No. of Samples in Ω_C(b) f_4 No. of Samples in Ω_C(c) f_6 No. of Samples in Ω_C

Fig. 5: Number of Samples in Critical Region

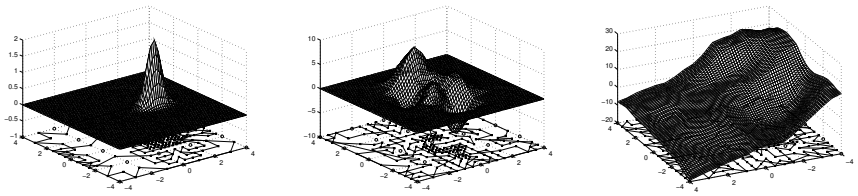

(a) $L_s^{\text{wTH}} \approx 170$, $\texttt{MSE} = 0.0002$ (b) $L_s^{\text{wTH}} \approx 186$, $\texttt{MSE} = 0.0190$ (c) $L_s^{\text{wTH}} \approx 194$, $\texttt{MSE} = 0.0552$

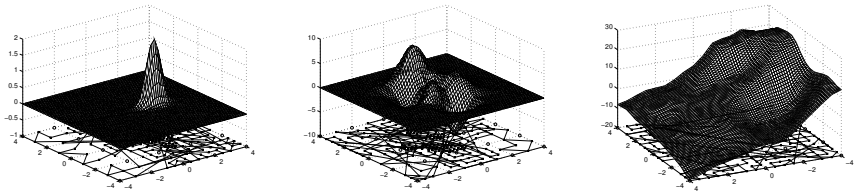

(d) $L_s^{\text{GR}} = 320$, $\texttt{MSE} = 0.0002$ (e) $L_s^{\text{GR}} \approx 337$, $\texttt{MSE} = 0.0141$ (f) $L_s^{\text{GR}} \approx 391$, $\texttt{MSE} = 0.0512$

Fig. 6: 256-Sample Reconstruction and Vehicle Trajectories GR and wTH: Left f_1, Middle f_4 and Right f_6

For most $\{\Delta t : \Delta t < T^{\text{LM}}\}$, all the other three algorithms are preferable to LM.

In the case of localized functions such as f_1, in which both $\mathcal{L}$ and $\mathcal{R}$ are low, the performance of GR is comparable to that of LM for high resolution recovery and wTH is superior to LM and offers significant savings in time (and hence energy). This is due to the fact that for such functions both the MSAS algorithms super-resolve the critical region with far fewer samples than non-adaptive algorithms (Fig. 5). GR, which maximizes sampling in the critical region, outperforms wTH initially. However, in later stages, the savings in distance traveled of wTH are of greater consequence than the savings accrued by GR in terms of number of samples, and wTH dominates the performance of GR.

For functions such as f_6 in which both the $\mathcal{L}$ and $\mathcal{R}$ are high, when $\tau_m = 0$, the savings in number of samples accrued by GR is offset by the high value of distance traveled per sample (Fig. 4). Its performance, while better than LM for a significant percent of T^{LM}, is inferior to both wTH and SR. This implies that in cases where the errors due to lack of coverage dominate the errors due to lack of resolution, seeking feature regions at the cost of distance traveled, offers no benefit, and algorithms such as SR and wTH which balance coverage with resolution are preferable. The performance of wTH dominates that of SR since it actively samples critical region at a higher rate than SR.

For the case of functions of such as f_4 in which both the $\mathcal{L}$ and $\mathcal{R}$ are medium, evaluation of the relative performance of the algorithms is congruent with the discussion above, and falls between the extreme cases represented by f_1 and f_6. Thus $T^{\text{LM}}(f_1) < T^{\text{LM}}(f_4) < T^{\text{LM}}(f_6)$. Similarly, while both MSAS algorithms are superior to SR, as in the case of

f_1, wTH outperforms GR as in f_6 since the relative errors due to coverage are more significant in f_4 than in f_1. Also, the range of Δt for which MSAS dominates LM is between the corresponding ranges for the case of f_1 and f_6. Similarly, while GR dominates SR for f_1, it is inferior to SR in the case of f_6. In the case of f_4 with respect to SR, eventually, the travel costs of GR overwhelm any relative benefits of sampling in the critical region and SR dominates GR.

C. Effect of Finite Measurement Time

Many missions are characterized by $\tau_m > 0$ and $v < \infty$. For missions with such profiles, the relative performance of the algorithms represents a balance between measurement costs and travel costs. The effect of finite τ_m can be analyzed based on the information contained in Fig. 3. Let T_α be the time taken to achieve α percent error for the $\kappa = 0$ case:

$$T_\alpha = \frac{L_\alpha}{v} + N_\alpha \tau_m \tag{4}$$

where, N_α is the number of samples taken to achieve α percent error and, L_α the corresponding distance traveled. The N_α and L_α for three error levels are tabulated in Table III. Three α levels are considered: 0.95, 0.995 and 0.999 which respectively correspond to approximately 15%, 45% and 70% of the total samples taken by wTH for the reconstruction of f_6 and thus may be assumed to represent a low, medium and high sample rate reconstruction.

The information in this table is congruent with previous discussion. For example, for f_1, $N^{\text{GR}}_{.999} < N^{\text{LM}}_{.999}$ and $L^{\text{GR}}_{.999} < L^{\text{LM}}_{.999}$, consequently $T^{\text{GR}}_{.999} < T^{\text{LM}}_{.999}$. In contrast, for f_6, LM dominates GR since, $N^{\text{GR}}_{.999} = 759, N^{\text{LM}}_{.999} = 1079$ and $L^{\text{GR}}_{.999} = 871.71, L^{\text{LM}}_{.999} = 273.67$ and therefore $T^{\text{LM}}_{.999} < T^{\text{GR}}_{.999}$.

However, if the mission characteristic, κ, were at least as large as:

$$\kappa^* = \frac{L^{\text{GR}}_\alpha - L^{\text{LM}}_\alpha}{N^{\text{LM}}_\alpha - N^{\text{GR}}_\alpha} = 1.9189, \tag{5}$$

then $T^{\text{GR}}_\alpha \leq T^{\text{LM}}_\alpha$ and GR would dominate LM. For a nominal vehicle speed of 3 knots (5.556 kms/hr), if the τ_m per sample is at least $\tau^*_\alpha = 20.72$ minutes per sample, then GR dominates LM at $\alpha = .999$. Similarly, if the mission required a τ_m of greater than 3.27 minutes per sample then wTH will dominate LM at error level $\alpha = .999$. The corresponding t^*_α for SR is 30.06 minutes per sample. Thus if the τ_m at each site were atleast 3.27 minutes, then wTH would dominate the performance of a distance ordered LM at an $\alpha = .999$ for f_6.

The critical missions characteristics κ^* and the corresponding measurement times τ^*_m for a nominal vehicle speed of 3 knots are shown in Table IV. Fig. 7 shows the T_α vs. κ characteristic of algorithms at the 3 error levels considered. The $\kappa^* > 0$ values in Table IV correspond to the abscissae where the respective curves intersect the LM line.

As is seen in that table, the mission characteristic required for wTH to dominate LM sampling is the much lower than that of GR and SR. For localized functions, wTH dominates LM at all the error levels and the entire set of possible mission profiles $\kappa^* \geq 0$ is feasible. This means that even for missions in which the experimental variable can be measured instantaneously, wTH outperforms LM. For non-localized functions, wTH dominates LM at low resolution. For higher resolutions, the value of κ^* required to dominate LM is small when compared to GR and SR, thus making wTH a feasible alternative to LM and SR for a wider range of missions.

Further, the rate of increase in T_α as κ increases is much lower for wTH than LM due to the large number of samples required for LM to achieve a given level of error. Since in LM improvement in resolution can only be achieved by increasing the sample rate, for a given vehicle speed, the time required for LM to achieve a given level of error increases much more rapidly than wTH as the τ_m increases.

ACKNOWLEDGMENTS

This work has been conducted in conjunction with the Center for Automation Technology at Rensselaer Polytechnic Institute and the Autonomous Undersea Systems Institute, Lee, NH.

REFERENCES

[1] M. Babin, J. J. Cullen, C. S. Roesler, P. L. Donaghay, G. J. Doucette, M. Kahru, M. R. Lewis, C. A. Scholin, M. E. Sieracki, and H. M. Sosik. New Approaches and Technologies for Observing Harmful Algal Blooms. *Oceanography*, 18(2), 2005.

[2] M. A. Batalin and G. S. Sukhatme. Coverage, Exploration and Deployment by a Mobile Robot and Communication Network. *Telecommunication Systems*, 26(2):181–196, 2004.

[3] ECOM-3D. http://ompl.marine.usf.edu/tbmodel/ecom3d.htm.

[4] V. Hombal, A. Sanderson, and D.R. Blidberg. Adaptive multiscale sampling in robotic sensor networks. In *Proceedings of the 2009 IEEE/RSJ international conference on Intelligent robots and systems*, pages 122–128. IEEE Press, 2009.

[5] V. Hombal, A. C. Sanderson, and R. Blidberg. A non-parametric iterative algorithm for adaptive sampling and robotic vehicle path planning. *Intelligent Robots and Systems, 2006 IEEE/RSJ International Conference on*, pages 217–222, Oct. 2006.

[6] N. E. Leonard, D. A. Paley, F. Lekien, R. Sepulchre, D. M. Fratantoni, and R. E. Davis. Collective motion, sensor networks, and ocean sampling. *Proceedings of the IEEE*, 95(1):48–74, Jan. 2007.

[7] P. A. Matthews. The Impact of Nonsynoptic Sampling on Mesoscale Oceanographic Surveys with Towed Instruments. *Journal of Atmospheric and Oceanic Technology*, 14(1):162–174, 1997.

[8] D.O. Popa, A.C. Sanderson, V.K. Hombal, R.J. Komerska, S.S. Mupparapu, R. Blidberg, and S.C. Chappel. Optimal sampling using singular value decomposition of the parameter variance space. *Intelligent Robots and Systems, 2005. (IROS 2005). 2005 IEEE/RSJ International Conference on*, 2005.

[9] M. Rixen and J. M. Beckers. A synopticity test of a sampling pattern in the Alboran Sea. *Journal of Marine Systems*, 35(1-2):111–130, 2002.

[10] A. Singh, R. Nowak, and P. Ramanathan. Active learning for adaptive mobile sensing networks. In *Proceedings of the fifth international conference on Information processing in sensor networks*, pages 60–68. ACM New York, NY, USA, 2006.

[11] S. Sokolov and S. R. Rintoul. Some Remarks on Interpolation of Nonstationary Oceanographic Fields. *Journal of Atmospheric and Oceanic Technology*, 16(10):1434–1449, 1999.

[12] Z. Song, Y.Q. Chen, C.R. Sastry, and N.C. Tas. *Optimal Observation for Cyber-physical Systems: A Fisher-information-matrix-based Approach*. Springer Verlag, 2009.

[13] C. Tricaud and Y.Q. Chen. Optimal mobile actuator/sensor network motion strategy for parameter estimation in a class of cyber physical systems. In *ACC'09: Proceedings of the 2009 conference on American Control Conference*, pages 367–372. IEEE Press, 2009.

[14] J. S. Willcox, J. G. Bellingham, Y. Zhang, and A. B. Baggeroer. Performance metrics for oceanographic surveys with autonomous underwater vehicles. *Oceanic Engineering, IEEE Journal of*, 26(4):711–725, Oct 2001.

α	0.950				0.995				0.999			
	wTH	GR	SR	LM	wTH	GR	SR	LM	wTH	GR	SR	LM
	No. of Samples Taken, N_α											
f_1	103	40	161	788	201	198	837	845	227	202	862	948
f_2	87	89	105	900	268	225	276	1083	661	524	816	1085
f_3	151	96	161	883	283	274	658	1083	606	565	839	1085
f_4	202	119	201	685	411	302	734	844	528	455	812	878
f_5	452	378	728	909	568	425	1035	1080	570	431	1084	1080
f_6	159	145	213	940	495	393	626	1070	755	759	1013	1079
	Distance Traveled, L_α											
f_1	80.94	12.12	132.06	199.36	138.60	230.18	399.66	214.56	148.28	231.43	407.76	240.31
f_2	68.02	121.80	94.02	228.31	189.03	308.40	206.92	274.92	334.46	674.23	392.30	275.42
f_3	108.94	121.12	132.06	224.06	191.36	384.20	340.93	274.92	309.99	729.73	400.66	275.42
f_4	151.36	144.49	157.68	173.61	249.25	364.87	364.74	214.31	293.41	547.59	391.30	222.81
f_5	256.11	434.94	362.39	230.56	300.03	459.49	465.48	273.92	300.94	463.65	481.69	273.92
f_6	124.89	196.51	166.88	238.31	281.28	509.06	328.97	271.17	370.47	887.71	457.38	273.67

TABLE III: No. of Samples Taken and Distance Traveled to α percent error.

α	0.950			0.995			0.999		
	wTH	GR	SR	wTH	GR	SR	wTH	GR	SR
	κ^*								
f_1	0.00	0.00	0.00	0.00	0.02	23.14	0.00	0.00	1.95
f_2	0.00	0.00	0.00	0.00	0.04	0.00	0.14	0.71	0.43
f_3	0.00	0.00	0.00	0.00	0.14	0.16	0.07	0.87	0.51
f_4	0.00	0.00	0.00	0.08	0.28	1.37	0.20	0.77	2.55
f_5	0.06	0.38	0.73	0.05	0.28	4.26	0.05	0.29	0.00
f_6	0.00	0.00	0.00	0.02	0.35	0.13	0.30	1.92	2.78
	τ_m^* (minutes), $v = 5.556$km/hr								
f_1	0.00	0.00	0.00	0.00	0.26	249.85	0.00	0.00	21.03
f_2	0.00	0.00	0.00	0.00	0.42	0.00	1.50	7.68	4.69
f_3	0.00	0.00	0.00	0.00	1.46	1.68	0.78	9.43	5.50
f_4	0.00	0.00	0.00	0.87	3.00	14.77	2.18	8.29	27.57
f_5	0.60	4.16	7.87	0.55	3.06	45.97	0.57	3.16	0.00
f_6	0.00	0.00	0.00	0.19	3.79	1.41	3.23	20.72	30.06

TABLE IV: Critical Mission Characteristics and Measurement Times (LM baseline). Upper panel: Minimum mission characteristic required for an algorithm to dominate LM sampling at given α level. Lower Panel: The corresponding values for critical measurement times computed for a nominal vehicle speed.

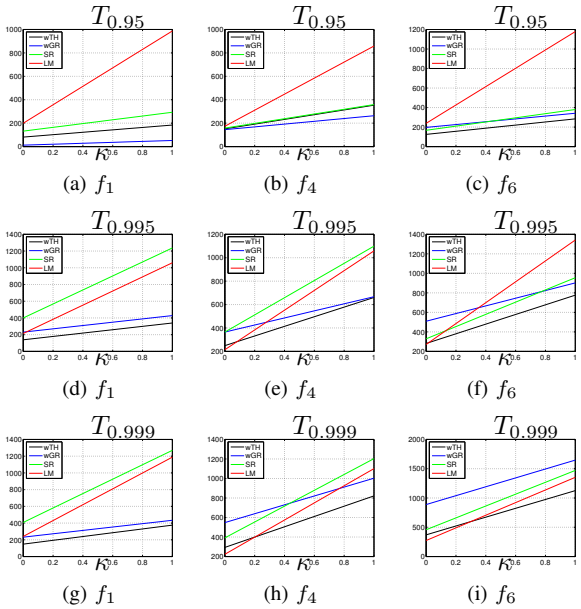

(a) f_1 (b) f_4 (c) f_6

(d) f_1 (e) f_4 (f) f_6

(g) f_1 (h) f_4 (i) f_6

Fig. 7: Effect of Measurement Time: T_α Vs τ_m